Supplementary Information: Universal scaling relation between the minimal conductivity and Hall conductivity in unpaired Dirac fermions

Bo Fu[1], Kai-Zhi Bai[2], Shi-Hao Bi[2], and Shun-Qing Shen[2,3]

[1]School of Sciences, Great Bay University, Dongguan 523000, China
[2]Department of Physics, The University of Hong Kong, Pokfulam Road, Hong Kong, China
[3]Department of Physics and State Key Laboratory of Optical Quantum Matter, The University of Hong Kong, Pokfulam Road, Hong Kong, China

March 11, 2026

Contents

1 Solution to self-consistent Born approximation at $E = 0$

The pair of self-consistent equations obtained from the SCBA framework reads

$$\Sigma_0 = -\gamma E' \ln\left[\frac{-E_c^2}{E'^2 - m'^2}\right]; \quad \Sigma_z = -\gamma m' \ln\left[\frac{-E_c^2}{E'^2 - m'^2}\right], \tag{S1}$$

which corresponds to the self-energy of gapped Dirac bands $\Sigma^R = \Sigma_0\sigma_0 + \Sigma_z\sigma_z$. The renormalized energy and mass are defined self-consistently as $E' = E - \Sigma_0$ and $m' = m + \Sigma_z$. At the charge neutrality point with $E = 0$, the set of equations simplifies to

$$\Sigma_0 = \gamma\Sigma_0 \ln\left[\frac{-E_c^2}{\Sigma_0^2 - (m + \Sigma_z)^2}\right]; \quad \Sigma_z = -\gamma(m + \Sigma_z) \ln\left[\frac{-E_c^2}{\Sigma_0^2 - (m + \Sigma_z)^2}\right], \tag{S2}$$

and one sees two possibilities: $\Sigma_0 = 0$ or $\Sigma_0 \neq 0$.

When $\Sigma_0 \neq 0$, it is reasonable to set Σ_0 as purely imaginary with $\eta = -\Im\Sigma_0$ and Σ_z as purely real with $m' = m + \Sigma_z$. The equations then become

$$1 = \gamma \ln\frac{E_c^2}{\eta^2 + m'^2}; \quad m - m' = -\gamma m' \ln\frac{E_c^2}{\eta^2 + m'^2},$$

whose ratio leads to $\frac{1}{m'-m} = -\frac{1}{m'}$ and $m' = \frac{m}{2}$, meaning that the effective gap is negatively renormalized to half its bare value. Correspondingly, we have

$$\eta = \sqrt{E_c^2 e^{-\frac{1}{\gamma}} - \frac{m^2}{4}} = \frac{1}{2} m_c \sqrt{1 - \left(\frac{m}{m_c}\right)^2},$$

where $m_c = 2E_c e^{-\frac{1}{2\gamma}}$. To maintain consistency with our assumption, we need $(m/m_c)^2 < 1$, which leads to the critical disorder strength $\gamma > \gamma_c = \left(2 \ln \frac{2E_c}{|m|}\right)^{-1}$.

On the other hand, when $\gamma < \gamma_c$, we turn to the $\Sigma_0 = 0$ case and find a transcendental equation for Σ_z:

$$1 = 2\gamma f \left(\ln \frac{E_c}{m} + 1 - \ln f\right), \quad f = \frac{m'}{m}.$$

Two limits are easy to verify: (i) at $\gamma = \gamma_c$, $m' = \frac{m}{2}$ satisfies the equation; (ii) at $\gamma = 0$, $m' = m$ satisfies the equation, meaning $\Sigma_z = \Sigma_0 = 0$ with no correction.

The numerical calculation is presented in the main text.

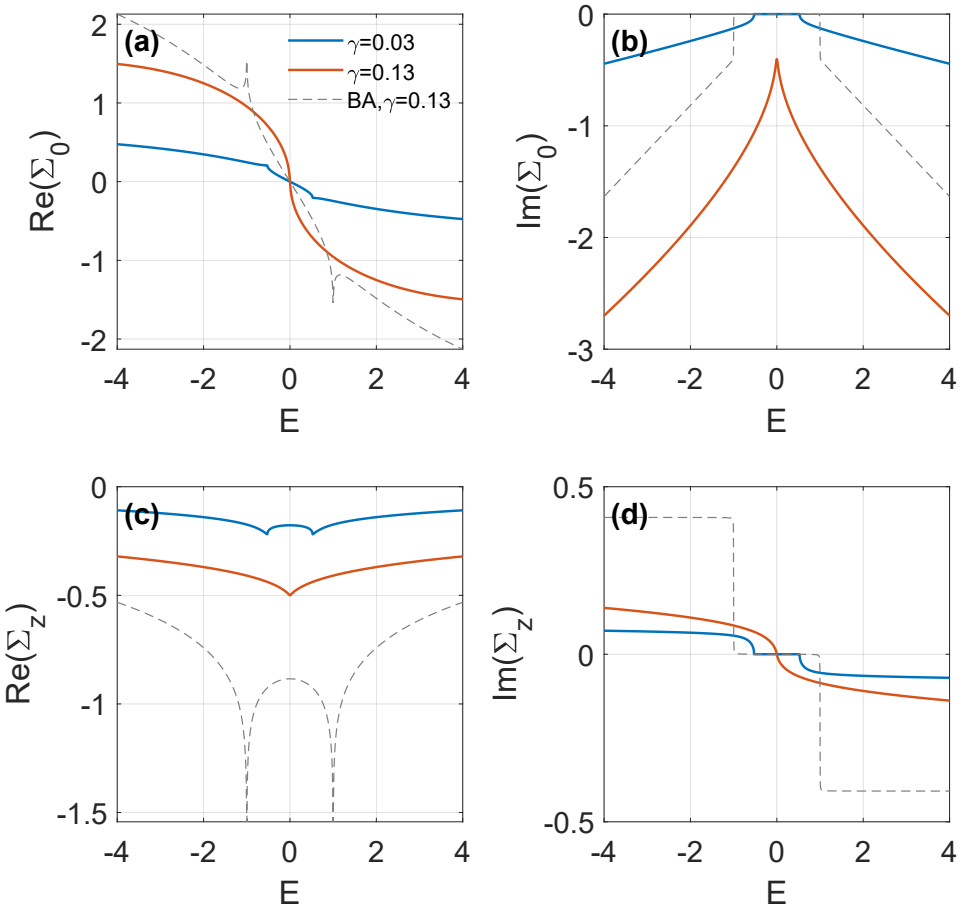

Figure S1: Real and imaginary parts of the self-energies Σ_0 and Σ_z as a function of energy E for $\gamma = 0.03$ (below the critical disorder γ_c) and $\gamma = 0.13$ (above γ_c). Results from the Born approximation with $\gamma = 0.13$ (dashed lines) are shown for comparison. The bare gap $m = 1$ is used as the energy unit.

2 Vertex correction to conductivities

The Kubo formula for electrical conductivity is derived from the current-current correlation function, which is defined in imaginary time at finite temperature

$$\chi_{ab}(i\omega_l) = \frac{e^2}{V}\int_0^\beta d\tau e^{i\omega_l\tau}\langle T_\tau v_a(\tau)v_b(0)\rangle$$

where $v_a = \frac{1}{\hbar}\partial_{k_a}H$ is the velocity operator for a direction, $i\omega_l = i2\pi l/\beta$ is the bosonic Matsubara frequency with $\beta = 1/T$ the inverse temperature, and $\langle T_\tau \cdots\rangle$ denotes the thermal and time-ordered expectation value. The electrical conductivity is obtained via analytic continuation $i\omega_m \to \omega + i0$ of the correlation function:

$$\sigma_{ab}(\omega) = i\frac{\chi_{ab}(\omega+i0)}{\omega}.$$

Within the framework of diagrammatic perturbation theory for a system with impurity scattering, the correlation function can be expressed as

$$\chi_{ab}(i\omega_l) = \frac{e^2}{\beta V}\sum_{\mathbf{k},ip_n}\mathrm{Tr}[v_a\mathcal{G}(\mathbf{k},ip_n)\widetilde{v}_b(ip_n,ip_n+i\omega_l)\mathcal{G}(\mathbf{k},ip_n+i\omega_l)]$$

where $ip_n = i(2n+1)\pi/\beta$ is a fermionic Matsubara frequency, $\mathcal{G}(\mathbf{k},ip_n)$ is the dressed single-particle Green's function calculated within the SCBA, and $\widetilde{v}_b$ is the renormalized vertex, which includes corrections from impurity scattering.

For a generic massive Dirac system with Hamiltonian $H = v\mathbf{k}\cdot\boldsymbol{\sigma} + m\sigma_z$, the SCBA Green's function is:

$$\mathcal{G}(\mathbf{k},ip_n) = \frac{1}{ip_n' - v\mathbf{k}\cdot\boldsymbol{\sigma} - m'(ip_n)\sigma_z} = -\frac{ip_n' + v\mathbf{k}\cdot\boldsymbol{\sigma} + m_n'\sigma_z}{p_n'^2 + v^2k^2 + m_n'^2}.$$

The quantities $ip_n' = ip_n - \Sigma_0(ip_n)$ and $m_n' = m + \Sigma_z(ip_n)$ are the renormalized energy and mass, respectively, incorporating the impurity self-energy.

The self-energies are calculated within the self-consistent Born approximation (SCBA), as diagrammatically represented in Fig. 2(a1) of the main text. The retarded self-energies Σ_0 and Σ_z are shown in Fig. S1(a-d) for disorder strengths below and above the critical value γ_c. For comparison, we also plot results from the Born approximation for a specific value of γ. While the overall amplitude of the self-energy varies with γ, the key qualitative features—such as the positions of singularities in the real part (at $E = \pm m$) and the energy range where they vanish in the imaginary part ($|E| < |m|$)—remain unchanged. The real and imaginary parts exhibit opposite parity in energy, a consequence of the Kramers-Kronig relations. Above γ_c, the band gap is smeared, as evidenced by the finite $\mathrm{Im}\Sigma_0$ at $E = 0$ in panel (b). Furthermore, the mass renormalization $\mathrm{Re}\Sigma_z$ (panel (c)) always has the sign of the bare mass m, reducing the effective mass and thereby promoting the insulator-to-metal transition.

The renormalized vertex is expressed as $\widetilde{v}_b = v_b + \delta v_b$, where v_b is the bare vertex and δv_b is the impurity-induced correction. This correction is found by solving the Bethe-Salpeter equation, which sums the ladder diagram series self-consistently (as illustrated in Fig. 2(a2)):

$$\delta v_b(ip_n,ip_n+i\omega_l) = \bar{v}_b(ip_n,ip_n+i\omega_l) + 4\pi v^2\gamma\sum_{\mathbf{k}}\mathcal{G}(\mathbf{k},ip_n)\delta v_b(ip_n,ip_n+i\omega_l)\mathcal{G}(\mathbf{k},ip_n+i\omega_l). \quad \text{(S3)}$$

The inhomogeneous term $\bar{v}_b$ represents the first-order correction in impurity density. For the $b = x$ direction, it evaluates to:

$$\begin{aligned}\bar{v}_x(ip_n,ip_n+i\omega_l) &= (4\pi v^2\gamma)\sum_{\mathbf{k}}\mathcal{G}(\mathbf{k},ip_n)v_x\mathcal{G}(\mathbf{k},ip_n+i\omega_l)\\ &= v(\mathcal{F}_{n,n+l}\sigma_x - \mathcal{R}_{n,n+l}\sigma_y)\end{aligned} \quad \text{(S4)}$$

where the scalar functions $\mathcal{F}$ and $\mathcal{R}$ are defined as

$$\mathcal{F}_{n,n+l} = \gamma \frac{p'_n p'_{n+l} + m'_n m'_{n+l}}{p'^2_{n+l} + m'^2_{n+l} - p'^2_n - m'^2_n} [\ln(p'^2_n + m'^2_n) - \ln(p'^2_{n+l} + m'^2_{n+l})],$$
$$\mathcal{R}_{n,n+l} = \gamma \frac{m'_{n+l} p'_n - m'_n p'_{n+l}}{p'^2_{n+l} + m'^2_{n+l} - p'^2_n - m'^2_n} [\ln(p'^2_n + m'^2_n) - \ln(p'^2_{n+l} + m'^2_{n+l})]. \tag{S5}$$

A similar result holds for $\bar{v}_y = \mathcal{F}_{n,n+l}\sigma_y + \mathcal{R}_{n,n+l}\sigma_x$.

Assuming an ansatz for the vertex function $\delta v_x = \sum_{i=0,x,y,z} c_{xi}\sigma_i$ and using symmetry arguments (odd functions in $\mathbf{k}$ vanish upon integration), we find $c_{x0} = c_{xz} = 0$. Substituting into the Bethe-Salpeter equation (S3) and matching coefficients for σ_x and σ_y yields the solutions:

$$\widetilde{v}_x(ip_n, ip_n + i\omega_l) = v \frac{(1 - \mathcal{F}_{n,n+l})\sigma_x - \mathcal{R}_{n,n+l}\sigma_y}{(1 - \mathcal{F}_{n,n+l})^2 + \mathcal{R}^2_{n,n+l}} \tag{S6}$$

To evaluate the DC conductivity tensor, we compute the vertex functions $\mathcal{F}$ and $\mathcal{R}$ in different scattering channels: RR and AA channels need expansions to $O(\omega^1)$ while the AR channel only requires $O(\omega^0)$ terms. The results are:

$$\mathcal{F}^{RR}(E, E+\omega) = \mathcal{F}^{AA}(E, E+\omega) = -\gamma + O(\omega^2),$$
$$\mathcal{R}^{RR}(E, E+\omega) = \gamma i \frac{(-\partial_E E' m' + \partial_E m' E')}{m'^2 - E'^2}\omega + O(\omega^2),$$
$$\mathcal{R}^{AA}(E, E+\omega) = \gamma i \frac{(-\partial_E E'^* m'^* + \partial_E m'^* E'^*)}{m'^{*2} - E'^{*2}}\omega + O(\omega^2),$$
$$\mathcal{F}^{AR}(E, E+\omega) = -\gamma \frac{|m'|^2 - |E'|^2}{\mathrm{Im}(m'^2 - E'^2)} \mathrm{Im}\ln(m'^2 - E'^2),$$
$$\mathcal{R}^{AR}(E, E+\omega) = \gamma \frac{2\mathrm{Im}(E'm'^*)}{\mathrm{Im}(m'^2 - E'^2)} \mathrm{Im}\ln(m'^2 - E'^2). \tag{S7}$$

Here $E' = E - \Sigma_0(E)$ and $m' = m + \Sigma_z(E)$ represent the renormalized energy and mass after including retarded self-energy corrections. The nonzero $\mathcal{F}^{RR}$ and $\mathcal{F}^{AA}$ terms lead to a renormalization of the velocity v. Substituting these into Eq. (S6) shows that the velocity in the Green's function should be rescaled as $v \to v/(1+\gamma)$.

In the zero-frequency DC limit ($\omega \to 0$), after performing analytic continuation and working in the retarded (R) and advanced (A) space, the conductivity formula becomes:

$$\sigma_{ab} = -\frac{e^2}{h}\mathrm{Re}\int_{-\infty}^{+\infty} dE \left\{ n_F(E)[\partial_\omega \Pi^{RR}_{ab}(E, E+\omega) - \partial_\omega \Pi^{AA}_{ab}(E, E+\omega)]|_{\omega\to 0} \right.$$
$$\left. + \partial_E n_F(E)[\Pi^{AR}_{ab}(E, E) - \Pi^{AA}_{ab}(E, E)] \right\}. \tag{S8}$$

Here, the kernel Π_{ab} is obtained by analytic continuation from its Matsubara counterpart (Fig. 2(a3)):

$$\Pi_{ab}(ip_n, ip_n + i\omega_l) = \int \frac{d^2\mathbf{k}}{(2\pi)^2} \mathrm{Tr}[v_a \mathcal{G}(\mathbf{k}, ip_n)\widetilde{v}_b \mathcal{G}(\mathbf{k}, ip_n + i\omega_l)]$$

Substituting the solved vertex function in Eq. (S6) leads to the explicit results:

$$\Pi_{yx}(ip_n, ip_n + i\omega_l) = -\frac{(1+\gamma)^2}{2\pi\gamma} \frac{\mathcal{R}_{n,n+l}}{(1 - \mathcal{F}_{n,n+l})^2 + \mathcal{R}^2_{n,n+l}},$$
$$\Pi_{xx}(ip_n, ip_n + i\omega_l) = -\frac{(1+\gamma)^2}{2\pi\gamma} \left\{ 1 - \frac{1 - \mathcal{F}_{n,n+l}}{(1 - \mathcal{F}_{n,n+l})^2 + \mathcal{R}^2_{n,n+l}} \right\}. \tag{S9}$$

Substituting these results into the conductivity formulas yields:

$$\begin{aligned}
\sigma_{xx} &= \frac{e^2}{h}\mathrm{Re}[\Pi^{AR}_{xx}(E,E) - \Pi^{AA}_{xx}(E,E)] \\
&= \frac{e^2(1+\gamma)^2}{2\pi h\gamma}\left\{-\frac{1}{1+\gamma} + \frac{1-\mathcal{F}^{AR}}{(1-\mathcal{F}^{AR})^2 + (\mathcal{R}^{AR})^2}\right\}, \\
\sigma_{yx} &= -\frac{e^2}{h}\int_{-\infty}^{\mu} dE\mathrm{Re}[\partial_\omega \Pi^{RR}_{yx}(E,E+\omega) - \partial_\omega \Pi^{AA}_{yx}(E,E+\omega)]|_{\omega\to 0} \\
&\quad + \frac{e^2}{h}\mathrm{Re}[\Pi^{AR}_{yx}(E,E) - \Pi^{AA}_{yx}(E,E)] \\
&= -\frac{e^2}{h}\frac{1}{\pi}\int_{-\infty}^{\mu} d\epsilon \mathrm{Im}\frac{(-\partial_E E' m' + \partial_E m' E')}{m'^2 - E'^2} \\
&\quad - \frac{(1+\gamma)^2}{2\pi\gamma}\frac{e^2}{h}\mathrm{Re}\left[\frac{\mathcal{R}^{AR}}{(1-\mathcal{F}^{AR})^2 + (\mathcal{R}^{AR})^2}\right].
\end{aligned} \tag{S10}$$

For Dirac fermion systems, once disorder drives the system into the intermediate metallic phase ($\gamma > \gamma_c$), the scattering rate $|\mathrm{Im}\Sigma^R_0(0)|$ becomes finite. The transport behavior depends crucially on energy E relative to the scattering rate, leading to two distinct regimes: (i) weak scattering regime $E \gg m, \eta$ and (ii) strong scattering regime $E \sim 0 \lesssim m, \eta$.

2.1 Weak Scattering Regime

In this regime, quasiparticles remain well-defined with energy scales significantly exceeding both the mass gap and disorder broadening. Here, RR and AA channel contributions are negligible. The self-energy simplifies to $E' \simeq E + i\pi\gamma E$ and $m' = m - i\pi\gamma m$. Thus, $\mathrm{Im}\ln(m'^2 - E'^2) = -\pi\Theta(|E| - |m|)$ where $\Theta(x)$ is the Heaviside step function. The vertex functions become:

$$\begin{aligned}
\mathcal{F}^{AR}(E, E+\omega) &\simeq \frac{E^2 - m^2}{2(m^2+E^2)}\Theta(|E| - |m|), \\
\mathcal{R}^{AR}(E, E+\omega) &\simeq 2\gamma\pi\frac{mE}{m^2+E^2}\Theta(|E| - |m|).
\end{aligned} \tag{S11}$$

To leading order in γ, the renormalized vertex in the RA channel reads $\widetilde{v}^{AR}_x = v\Lambda_W\sigma_x$ where $\Lambda_W = \frac{2(E^2+m^2)}{E^2+3m^2}$ is the vertex correction factor that recovers the well-known factor-of-2 enhancement for massless Dirac fermions. The resulting longitudinal conductivity σ_{xx} takes a generalized Drude form:

$$\sigma_{xx} = \frac{e^2}{h}\mathrm{Re}\Pi^{AR}_{xx} = \Lambda_W\sigma_{\mathcal{D}}$$

where $\sigma_{\mathcal{D}} = e^2\nu\mathcal{D}$ satisfies the Einstein relation. Here, $\nu = \frac{E}{2\pi v^2}$ is the density of states and $\mathcal{D} = \frac{v^2}{2}\frac{E^2-m^2}{E^2}\tau$ is the diffusion constant with relaxation time $\tau = \frac{1}{2\pi\gamma}\frac{E}{E^2+m^2}$.

The Hall conductivity σ_{yx} in this regime simplifies to:

$$\sigma_{yx} = \frac{e^2}{h}\mathrm{Re}\Pi^{AR}_{yx} = -\frac{e^2}{h}\frac{4mE(m^2+E^2)}{(E^2+3m^2)^2}.$$

This Hall conductivity separates into intrinsic and disorder-induced corrections from side-jump and skew-scattering parts for Gaussian disorder correlations.

2.2 Strong Scattering Regime

This regime represents the disorder-dominated limit where the system's energy scale E lies well below the disorder-induced broadening $\eta = |\mathrm{Im}\Sigma^R_0(0)|$. Here, disorder physics becomes non-perturbative and

qualitatively different from conventional metallic behavior. We have $E' \simeq E + i\eta$ with $E \ll \eta$ and $m' = m$. Thus: $\mathrm{Im}\ln(m'^2 - E'^2) \approx -\frac{2\eta E}{m^2+\eta^2}$. Unlike the weak-scattering case where RR and AA channels could be neglected, in the strong-scattering regime all three channels (RR, AA, and AR) contribute significantly. When η is comparable to or larger than $|m|$, the retarded and advanced Green's functions have substantial overlap even at zero energy separation, making products like $\mathcal{G}^R\mathcal{G}^R$ and $\mathcal{G}^A\mathcal{G}^A$ non-negligible. The vertex functions in this regime become:

$$\begin{aligned} \mathcal{F}^{AR} &\simeq \gamma \frac{\eta^2 - m^2}{m^2 + \eta^2}, \\ \mathcal{R}^{AR} &\simeq \gamma \frac{2\eta m}{m^2 + \eta^2}. \end{aligned} \tag{S12}$$

These are completely independent of E to leading order, indicating universal behavior near the Dirac point.

The longitudinal conductivity with full vertex corrections is obtained from

$$\sigma_{xx} = \frac{e^2}{h}\mathrm{Re}[\Pi_{xx}^{AR}(0,0) - \Pi_{xx}^{AA}(0,0)]$$

After evaluation in the strong scattering regime, we obtain

$$\sigma_{xx} \approx \Lambda_S \sigma_0^* \tag{S13}$$

where $\sigma_0^* = \frac{e^2}{\pi h}$ is the bare minimal conductivity for a gapless Dirac fermion, and the longitudinal vertex correction factor is:

$$\Lambda_S = \frac{1 - \gamma^2}{(1-\gamma)^2 + (1+\gamma)^2\widetilde{m}^2}$$

with $\widetilde{m} = m/\eta$.

The Hall conductivity naturally decomposes into Fermi sea (quantum geometric) and Fermi surface (dissipative) components. The Fermi sea term σ_{yx}^{sea} (first term in Eq. (S8)) probes filled states below the Fermi level and reflects the integrated Berry curvature modified by disorder. Using:

$$[\partial_\omega \Pi_{yx}^{RR}(E, E+\omega) - \partial_\omega \Pi_{yx}^{AA}(E, E+\omega)]|_{\omega\to 0} = \frac{1}{\pi}\mathrm{Im}\frac{(-\partial_E E' m' + \partial_E m' E')}{m'^2 - E'^2}$$

and integrating over occupied states, we obtain:

$$\sigma_{yx}^{sea} = -\sigma_0^* \arctan \widetilde{m} \tag{S14}$$

which shows that vertex corrections do not affect this part of the conductivity.

Since the constant mass approximation $M(\mathbf{k}) = m$ holds only for energies $E < \hbar v k_c$, a high-energy regulator must be included for $E > \hbar v k_c$, where the mass takes the form $M(\mathbf{k}) = m_0 - b\mathbf{k}^2$. This regulator contributes an additional Fermi sea term $-\mathrm{sgn}(b)\frac{e^2}{2h}$. The total Fermi sea Hall conductivity thus becomes

$$\sigma_{yx}^{sea} = -\sigma_0^* \arctan \widetilde{m} - \mathrm{sgn}(b)\frac{e^2}{2h}.$$

The Fermi surface term $\sigma_{yx}^{surf} = \frac{e^2}{h}\mathrm{Re}(\Pi_{yx}^{AR} - \Pi_{yx}^{AA})$ (second term in Eq. (S8)) describes dissipative transport from states at the Fermi energy. In the strong-scattering regime, it simplifies to

$$\sigma_{yx}^{surf} \equiv -\sigma_0^* \frac{\widetilde{m}}{\widetilde{m}^2 + 1}\Xi \tag{S15}$$

where the vertex correction factor for the Fermi surface

$$\Xi = \frac{(1+\gamma)^2}{1 + \gamma^2 + 2\gamma\frac{\widetilde{m}^2 - 1}{\widetilde{m}^2 + 1}}$$

encodes non-perturbative ladder-type vertex corrections. This factor can significantly enhance or suppress the Hall response depending on the values of γ and m.

Combining both contributions, the total Hall conductivity in the strong-scattering regime reads

$$\sigma_{yx} = -\frac{e^2}{2h}\,\mathrm{sgn}(b) - \sigma_0^* \left\{ \arctan \widetilde{m} + \Xi \frac{\widetilde{m}}{\widetilde{m}^2+1} \right\}.$$

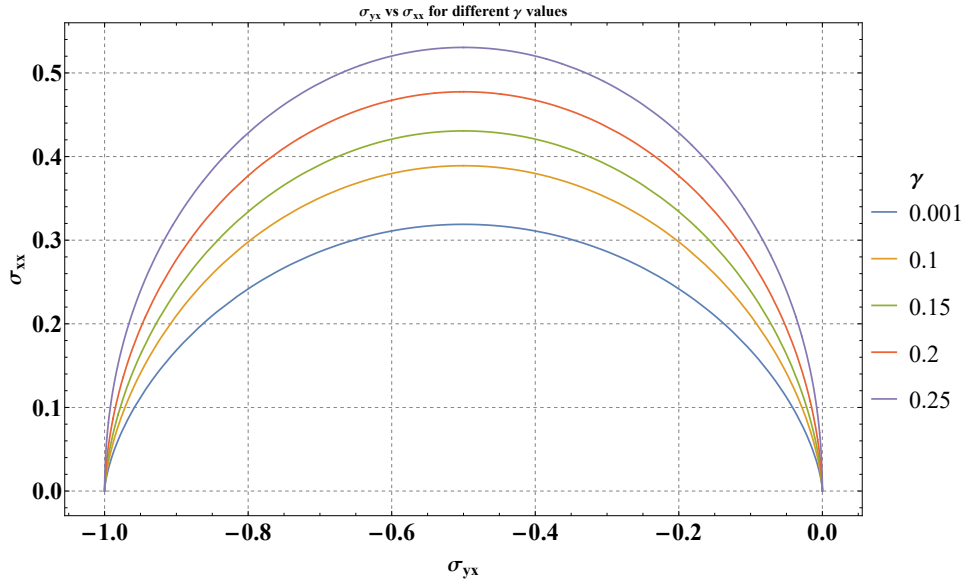

Figure S2: Vertex corrections for the σ_{yx} vs σ_{xx} near-elliptic relation across different γ computed from Eq. (S17) for $b > 0$.

2.3 Vertex Corrections to the Near-Elliptic Relation

By defining the vertex-corrected effective mass and minimal conductivity

$$\widetilde{m}_v = \frac{1+\gamma}{1-\gamma}\widetilde{m}, \quad \sigma^* = \frac{1+\gamma}{1-\gamma}\sigma_0^*$$

the Fermi-surface contributions in Eqs. (S13) and (S15) can be rewritten in a form identical to the uncorrected case:

$$\begin{aligned} \sigma_{xx} &= \sigma^* \frac{1}{1+\widetilde{m}_v^2}, \\ \sigma_{yx}^{surf} &= -\sigma^* \frac{\widetilde{m}_v}{\widetilde{m}_v^2+1}. \end{aligned} \tag{S16}$$

These components satisfy the relation

$$(\sigma_{xx} - \tfrac{1}{2}\sigma^*)^2 + (\sigma_{yx} - \sigma_{yx}^{sea})^2 = (\tfrac{1}{2}\sigma^*)^2 \tag{S17}$$

which follows from the intrinsic connection between the dissipative longitudinal and Hall conductivities arising from the Fermi surface in Dirac fermion systems.

We next express the Fermi-sea term σ_{yx}^{sea} in terms of σ_{xx}. This contribution has a topological origin, with two clear limits: (i) $\widetilde{m} \to \infty$, where $\sigma_{yx}^{sea} = -\frac{\mathrm{sgn}(b)+\mathrm{sgn}(m)}{2}\frac{e^2}{h}$ (quantized Hall regime), and (ii) $\widetilde{m} \to 0$, $\sigma_{yx}^{sea} = -\frac{\mathrm{sgn}(b)}{2}\frac{e^2}{h}$ (half-quantized regime). Using the relations $\gamma = \frac{\pi\sigma^*-1}{\pi\sigma^*+1}$ and $\widetilde{m} = \frac{\sigma_0^*}{\sigma^*}\widetilde{m}_v$, the Fermi-sea contribution to the Hall conductivity can be written in terms of σ_{xx} as

$$\sigma_{yx}^{sea} = \left(-\frac{\mathrm{sgn}(m)}{\pi} \arctan\left(\frac{\sigma_0^*}{\sigma^*} \sqrt{\frac{\sigma^*}{\sigma_{xx}} - 1} \right) - \frac{\mathrm{sgn}(b)}{2} \right) \frac{e^2}{h}. \tag{S18}$$

Substituting this into Eq. (S17) yields a near-elliptic relation between σ_{xx} and σ_{yx} of the same functional form as Eq. (1) in the main text, but with the characteristic conductivity σ^* now renormalized by vertex corrections. As shown in Fig. S2, the vertex correction modifies the near-elliptic relation with increasing disorder strength γ, producing two primary effects: (1) the peak conductivity rises above the intrinsic Dirac value $\sigma_0^* = e^2/\pi h$ and (2) the entire curve broadens significantly.

3 Quantum interference corrections from crossed diagrams

Having calculated vertex corrections from non-crossed ladder diagrams, we now evaluate the leading-order quantum interference contributions arising from crossed diagrams—specifically the Cooperon (X) and Ψ diagrams. These contributions represent coherent backscattering processes that are sensitive to phase coherence and become important in the strong scattering regime.

The contributions to conductivity from crossed diagrams shown in Fig. 2(a4) in the main text are given by:

$$\sigma_{xx}^{X} = \frac{e^2}{h}\mathrm{Re}(\Pi_{xx}^{X,AR} - \Pi_{xx}^{X,AA}), \quad \sigma_{xx}^{\Psi} = \frac{e^2}{h}\mathrm{Re}(\Pi_{xx}^{\Psi,AR} - \Pi_{xx}^{\Psi,AA})$$

where the polarization functions are defined as:

$$\begin{aligned}
\Pi_{ab}^{X}(ip_n, ip_n + i\omega_l) &= (4\pi v^2\gamma)^2 \int d^2\mathbf{r}\,\mathrm{Tr}[V_a(ip_n + i\omega_l, ip_n; \mathbf{r})\mathcal{G}(-\mathbf{r}, ip_n)V_b(ip_n, ip_n + i\omega_l; \mathbf{r})\mathcal{G}(-\mathbf{r}, ip_n + i\omega_l)], \\
\Pi_{ab}^{\Psi}(ip_n, ip_n + i\omega_l) &= (4\pi v^2\gamma)^2 \int d^2\mathbf{r}\,\{\mathrm{Tr}[V_a(ip_n + i\omega_l, ip_n; \mathbf{r})\mathcal{G}(-\mathbf{r}, ip_n)\mathcal{G}(\mathbf{r}, ip_n)V_b(ip_n, ip_n + i\omega_l; -\mathbf{r})] \\
&\quad + \mathrm{Tr}[V_a(ip_n + i\omega_l, ip_n; -\mathbf{r})V_b(ip_n, ip_n + i\omega_l; \mathbf{r})\mathcal{G}(-\mathbf{r}, ip_n + i\omega_l)\mathcal{G}(\mathbf{r}, ip_n + i\omega_l)]\}.
\end{aligned} \tag{S19}$$

The real-space vertex function with two adjacent Green functions is defined as:

$$V_a(ip_n, ip_n + i\omega_l; \mathbf{r}) = \int \frac{d^2\mathbf{k}}{(2\pi)^2} e^{i\mathbf{k}\cdot\mathbf{r}}\mathcal{G}(\mathbf{k}, ip_n)\widetilde{v}_a(ip_n, ip_n + i\omega_l)\mathcal{G}(\mathbf{k}, ip_n + i\omega_l). \tag{S20}$$

It is convenient to work directly in the retarded/advanced basis:

$$V_a^{ss'}(\mathbf{r}) = \int \frac{d^2\mathbf{k}}{(2\pi)^2}\mathcal{G}_{\mathbf{k}}^{s}\widetilde{v}_a^{ss'}\mathcal{G}_{\mathbf{k}}^{s'}e^{i\mathbf{k}\cdot\mathbf{r}}, \quad s, s' \in \{R, A\}. \tag{S21}$$

The corresponding real-space Green's function is

$$\mathcal{G}_{\mathbf{r}}^{s} = \int \frac{d^2\mathbf{k}}{(2\pi)^2}\mathcal{G}_{\mathbf{k}}^{s}e^{i\mathbf{k}\cdot\mathbf{r}}.$$

We focus on the strong-scattering regime, where the leading correction to the bare vertex in Eq. (S6) depends on γ. For the crossed diagrams, we therefore use the bare velocity vertex in Eq. (S20). Introducing the parameterization

$$\cos\varphi = \frac{m}{\zeta}, \quad \sin\varphi = \frac{\eta}{\zeta}$$

with $\zeta = \sqrt{m^2 + \eta^2}$, we obtain for the AR channel:

$$\begin{aligned}
V_x^{AR}(\mathbf{r}) &= \frac{r\zeta}{2\pi}\cos(\theta - \varphi)\left\{-\left[\cos(\varphi + \theta)\sigma_x + \sin(\theta + \varphi)\sigma_y\right]K_1(r\zeta) + iK_0(r\zeta)\,\sigma_z\right\}, \\
V_y^{AR}(\mathbf{r}) &= \frac{r\zeta}{2\pi}\sin(\theta - \varphi)\left\{-\left[\cos(\theta + \varphi)\sigma_x + \sin(\varphi + \theta)\sigma_y\right]K_1(\zeta r) + iK_0(\zeta r)\,\sigma_z\right\},
\end{aligned} \tag{S22}$$

and for the AA channel:

$$V_a^{AA}(\mathbf{r}) = \frac{\zeta r_a}{2\pi}\left\{(\sin\varphi + i\cos\varphi\sigma_z)K_0(\zeta r) - (\cos\theta\sigma_x + \sin\theta\sigma_y)K_1(r\zeta)\right\}. \tag{S23}$$

Here, $\theta = \arctan\frac{y}{x}$, and K_0, K_1 are modified Bessel functions of the second kind, which naturally appear due to the exponential decay of correlations in the presence of disorder broadening η. For the RA branch one takes $\eta \to -\eta$, which transforms $\varphi \to -\varphi$; a coordinate change $\mathbf{r} \to -\mathbf{r}$ simply corresponds to $\theta \to \theta + \pi$.

The retarded Green's function in real space is:

$$\begin{aligned}\mathcal{G}^R_{\pm\mathbf{r}} &= -(i\eta \mp iv\boldsymbol{\sigma}\cdot\boldsymbol{\nabla} + m\sigma_z)\int \frac{d^2\mathbf{k}}{(2\pi)^2}\frac{e^{\pm i\mathbf{k}\cdot\mathbf{r}}}{\eta^2 + v^2k^2 + m^2} \\ &= \frac{i\zeta}{2\pi v^2}[(-\sin\varphi + i\cos\varphi\sigma_z)K_0(\tfrac{\zeta r}{v}) \mp (\cos\theta\sigma_x + \sin\theta\sigma_y)K_1(\tfrac{\zeta r}{v})] \end{aligned} \tag{S24}$$

and the advanced Green's function is simply:

$$\mathcal{G}^A_{\pm\mathbf{r}} = \frac{i\zeta}{2\pi v^2}[(\sin\varphi + i\cos\varphi\sigma_z)K_0(\tfrac{\zeta r}{v}) \mp (\cos\theta\sigma_x + \sin\theta\sigma_y)K_1(\tfrac{\zeta r}{v})]. \tag{S25}$$

The $\cos\theta\sigma_x + \sin\theta\sigma_y$ terms reflect the spin–momentum locking characteristic of Dirac fermions.

Substituting the explicit expressions for $\mathcal{G}$ and V into the diagrammatic formulas, we obtain for the Cooperon diagram:

$$\begin{aligned}\Pi^{X,AR}_{xx} - \Pi^{X,AA}_{xx} &= (4\pi v^2\gamma)^2\int d^2\mathbf{r}\{\mathrm{Tr}[V^{AR}_x(\mathbf{r})\mathcal{G}^R_{-\mathbf{r}}V^{RA}_x(\mathbf{r})\mathcal{G}^A_{-\mathbf{r}}] - \mathrm{Tr}[V^{AA}_x(\mathbf{r})\mathcal{G}^A_{-\mathbf{r}}V^{AA}_x(\mathbf{r})\mathcal{G}^A_{-\mathbf{r}}]\} \\ &\approx (4\pi\gamma)^2\sin^2(\varphi)\int dx\frac{x^3K_1(x)^4}{4\pi^3}, \\ \Pi^{X,AR}_{yx} - \Pi^{X,AA}_{yx} &= (4\pi v^2\gamma)^2\int d^2\mathbf{r}\{\mathrm{Tr}[V^{AR}_y(\mathbf{r})\mathcal{G}^R_{-\mathbf{r}}V^{RA}_x(\mathbf{r})\mathcal{G}^A_{-\mathbf{r}}] - \mathrm{Tr}[V^{AA}_y(\mathbf{r})\mathcal{G}^A_{-\mathbf{r}}V^{AA}_x(\mathbf{r})\mathcal{G}^A_{-\mathbf{r}}]\} \\ &= (4\pi\gamma)^2\sin\varphi\cos\varphi\int dx\frac{x^3K_1(x)^4}{4\pi^3}, \end{aligned} \tag{S26}$$

and for the Ψ diagram:

$$\begin{aligned}\Pi^{\Psi,AR}_{xx} - \Pi^{\Psi,AA}_{xx} &= 2\times(4\pi v^2\gamma)^2\int d^2\mathbf{r}\{\mathrm{Tr}[V^{AR}_x(\mathbf{r})\mathcal{G}^R_{-\mathbf{r}}\mathcal{G}^R_{\mathbf{r}}V^{RA}_x(-\mathbf{r})] - \mathrm{Tr}[V^{AA}_x(\mathbf{r})\mathcal{G}^A_{-\mathbf{r}}\mathcal{G}^A_{\mathbf{r}}V^{AA}_x(-\mathbf{r})]\} \\ &\approx -2\times(4\pi\gamma)^2\cos^2\varphi\sin^2\varphi\int dx\frac{x^3K_1(x)^4}{2\pi^3}, \\ \Pi^{\Psi,AR}_{yx} - \Pi^{\Psi,AA}_{yx} &= 2\times(4\pi v^2\gamma)^2\int d^2\mathbf{r}\{\mathrm{Tr}[V^{AR}_y(\mathbf{r})\mathcal{G}^R_{-\mathbf{r}}\mathcal{G}^R_{\mathbf{r}}V^{RA}_x(-\mathbf{r})] - \mathrm{Tr}[V^{AA}_y(\mathbf{r})\mathcal{G}^A_{-\mathbf{r}}\mathcal{G}^A_{\mathbf{r}}V^{AA}_x(-\mathbf{r})]\} \\ &= 2\times(4\pi\gamma)^2(-\cos 2\varphi\sin 2\varphi)\int dx\frac{x^3K_1(x)^4}{8\pi^3}, \end{aligned} \tag{S27}$$

with $x = \zeta r$. The traces involve combinations of K_1^4, $K_1^2K_0^2$, and K_0^4. A high-energy cutoff E_c introduces a short-distance cutoff $x_c = \pi\zeta/E_c$. Because $K_1(x) \sim 1/x$ as $x \to 0$, the integral of $x^3K_1(x)^4$ dominates over those containing K_0; we therefore retain only the K_1^4 contributions. Defining the cutoff-dependent integral

$$\mathcal{I}\left(\frac{\zeta}{E_c}\right) = \frac{4}{\pi}\int_{\pi\zeta/E_c}^{\infty} dx\, x^3K_1(x)^4,$$

which for $\pi\zeta/E_c = 1/100$ gives $\mathcal{I} \approx 4.77$. Finally, we obtain the combined $X + \Psi$ corrections:

$$\begin{aligned}\sigma^{X+\Psi}_{xx} &= \frac{e^2}{h}\gamma^2\sin^2\varphi(1 - 4\cos^2\varphi)\mathcal{I}, \\ \sigma^{X+\Psi}_{yx} &= \frac{e^2}{h}\gamma^2\sin\varphi\cos\varphi(1 - 2\cos 2\varphi)\mathcal{I}. \end{aligned} \tag{S28}$$

For massless Dirac fermions ($m = 0$), we have $\cos\varphi = 0$ and $\sin\varphi = 1$. In this limit the transverse correction vanishes, the Ψ diagram gives no contribution to σ_{xx}, and the Cooperon yields a positive correction:

$$\sigma_{xx}^{X+\Psi} = \frac{e^2}{h}\gamma^2\mathcal{I}.$$

Note that this contribution is calculated in the strong-scattering regime, which is distinct from the usual weak-scattering evaluation. The resulting positive quantum-interference contribution to σ^* provides evidence for delocalization in the strong scattering regime of the PAS state.

4 Diverse flow diagrams in magnetic topological insulator sandwiches

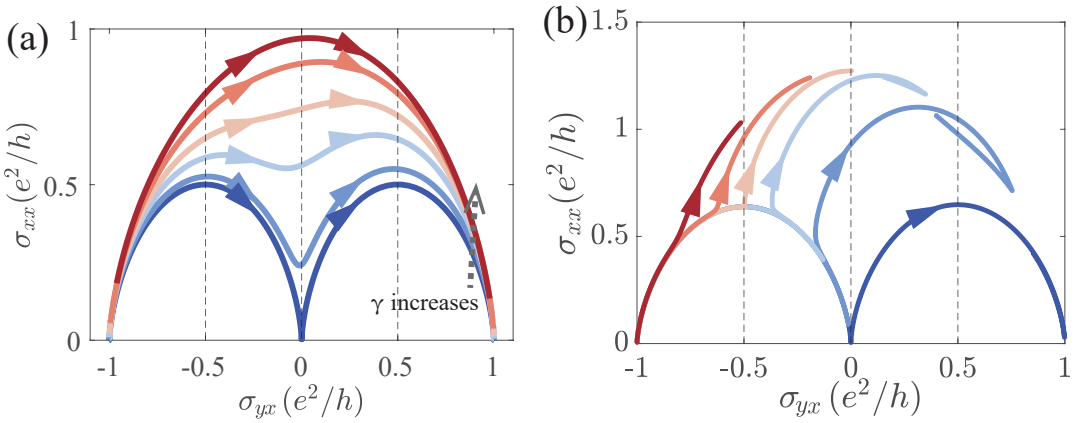

Figure S3: (a) Theoretical flow diagrams in the $(\sigma_{yx}, \sigma_{xx})$ plane under $B_\perp$. Arrows show increasing out-of-plane field $B_\perp$. The color lines from blue to red trace the evolution from the weak to the strong scattering limit with increasing scattering strength γ. (b) Resulting flow diagram under the application of $B_\parallel$. Arrows show increasing in-plane field $B_\parallel$.

Having fitted the experimental data in the limiting regimes in the main text, we now apply our theoretical framework to obtain analytical results for the crossover regimes.

The corresponding conductivity flow diagrams in Fig. S3(a) with the color gradient from blue to red trace the evolution from the weak to the strong scattering limit with increasing disorder strength γ. In the weak scattering limit (blue curve), where the disorder broadening is much smaller than the individual mass gaps, the trajectory of the flow forms a path comprised of two interconnected semi-elliptic segments that connect at the origin $(\sigma_{yx}, \sigma_{xx}) = (0, 0)$. In the strong scattering regime (red curve), significant disorder broadening smears out the intermediate axion insulator state, whose gap is relatively small. Consequently, the flow diagram collapses into a single semi-elliptic curve connecting the two insulating states (e.g., from $\sigma_{xy} = +\frac{e^2}{h}$ to $\sigma_{xy} = -\frac{e^2}{h}$), with a single peak in σ_{xx} at the gap-closing point. At intermediate disorder strengths, the flow diagram exhibits a crossover between these two limiting behaviors. This framework provides a natural explanation for the measured flow diagrams in samples of varying thickness [1].

The corresponding conductivity flow diagrams are shown in Fig. S3(b), with trajectories color-coded from red to blue as the fixed $B_\perp$ value changes from positive to negative. For $B_\perp = 0$, the distinct coercive fields cause the surface Zeeman fields to orient oppositely under $B_\parallel$, rendering one surface gapless ($m_b = 0$) while the other stays gapped ($m_t \neq 0$). The resulting conductivity flow [orange line in Fig. S3(b)] exhibits a distinct two-stage evolution: in the first stage, the system flows from its initial normal insulating state toward a PAS state characterized by a finite longitudinal conductivity and a half-quantized Hall conductivity; in the second stage, the net conductivity then follows an anomalous flow trajectory, which can be understood as the superposition of the conventional flow for a massive Dirac band and the constant background contribution from the established parity anomalous semimetal state. For fixed $B_\perp > 0$ (red line), both surfaces remain gapped, and the broken parity symmetry prevents the flow from

reaching the half-quantized σ_{xy} point. For $B_\perp < 0$ (blue line), the $B_\parallel$-induced mass inversion leads to a flow resembling that of varying $B_\perp$. At large $B_\parallel$, both Zeeman fields are forced nearly in-plane, driving the system to a Dirac semimetal phase with $(\sigma_{yx}, \sigma_{xx}) = (0, \sigma_t^* + \sigma_b^*)$. Our theory provides excellent agreement with the experimental data obtained under in-plane magnetic fields [2, 3, 4].

References

[1] Ruoxi Zhang, Yi-Fan Zhao, Ling-Jie Zhou, Deyi Zhuo, Zi-Jie Yan, Chao-Xing Liu, Moses H. W. Chan, Chui-Zhen Chen, and Cui-Zu Chang. Interlayer exchange coupling induced critical-metal-to-insulator phase transition in quantum anomalous hall insulators. *Phys. Rev. B*, 112:125402, Sep 2025. doi: 10.1103/6myc-8pr9. URL https://link.aps.org/doi/10.1103/6myc-8pr9.

[2] Deyi Zhuo, Bomin Zhang, Humian Zhou, Han Tay, Xiaoda Liu, Zhiyuan Xi, Chui-Zhen Chen, and Cui-Zu Chang. Half-quantized chiral edge current in a c= 1/2 parity anomaly state. *Physical Review Letters*, 136(1):016601, 2026.

[3] Binbin Wang, Jiayuan Hu, Bo Fu, Jiaqi Li, Yunchuan Kong, Kai-Zhi Bai, Shun-Qing Shen, and Di Xiao. Parity anomalous semimetal with minimal conductivity induced by an in-plane magnetic field. *arXiv preprint arXiv:2511.02446*, 2025.

[4] Ting-Hsun Yang, Yaochen Li, Peng Zhang, Yueh-Ting Yao, Hung-Yu Yang, Qingyuan Shu, Eun Sang Choi, Kin Wong, Tay-Rong Chang, Gang Qiu, et al. In-plane field induced half quantized hall conductivity in trilayer magnetic topological insulator. *Advanced Materials*, page e10754, 2025.